Int. J. Heat Mass Transfer Vol. 27, No. 12, pp. 2297–2306, 1984
Printed in Great Britain

0017 9310/84 $3.00 + 0.00

Impingement heat transfer at a circular cylinder due to an offset or non-offset slot jet

E. M. SPARROW and A. ALHOMOUD
Department of Mechanical Engineering, University of Minnesota, Minneapolis, MN 55455, U.S.A.

(*Received* 26 *January* 1984 *and in revised form* 2 *April* 1984)

Abstract—Heat transfer coefficients were measured on a circular cylinder subjected to the crossflow impingement of a slot jet. In one set of experiments, the symmetry plane of the jet was aligned with the axis of the cylinder, while in other experiments the jet was offset from the cylinder. In addition to the offset, parametric variations were also made for the width of the jet-inducing slot, the distance between the slot and the cylinder, and the Reynolds number. Supplementary flow visualization experiments showed that even in the presence of offset, the jet impinged on the cylinder, although not at the cylinder apex as in the aligned case. It was found that the heat transfer coefficient increased with slot width and Reynolds number but decreased with slot-to-cylinder separation distance and offset. The effect of offset is accentuated for narrow slots and at small slot-to-cylinder separation distances. The largest measured offset-related reduction in the heat transfer coefficient was slightly in excess of 50%.

INTRODUCTION

THE HIGH heat transfer coefficients associated with impinging gas jets has encouraged their use in a broad range of industrial applications. These applications include, for example, the drying of textiles, paper, veneer, and film materials and the annealing of metal and plastic sheets. There are numerous jet and impingement surface configurations which may be respectively employed to achieve various heat transfer objectives. Many of these configurations are described in a recent review article [1] which constitutes the most comprehensive survey of jet-impingement heat transfer presently available.

The research reported here is concerned with the impingement of a slot jet on a circular cylinder situated in crossflow with respect to the jet. Despite its practical relevance, this configuration has been only sparsely investigated in the literature [2–4] and is not included in the aforementioned survey article.

Figure 1 has been prepared to illustrate the physical situation that is the subject of the present research, which is experimental in nature. The figure shows a slot of width W into which air is drawn from a large upstream space. The flow separates from the sharp forward edges of the slot and thereby forms a two-dimensional (2-D) free jet (i.e. a slot jet). A circular cylinder of diameter D positioned in crossflow to the jet serves as the impingement surface. The cylinder is situated at a distance S from the origin of the jet. Its center may be offset by the distance E (eccentricity) from the geometric symmetry plane of the slot jet. The two-dimensionality of the flow over the instrumented portion of the cylinder was verified by supplementary flow visualization studies.

Measurements were made of the average heat transfer coefficient for the cylinder as a function of the geometrical and fluid flow parameters. As can be seen in Fig. 1, there are four dimensions that specify the problem: D, E, S, and W. These quantities can be cast into the dimension ratios W/D, S/D, and E/D, and it is these three dimensionless groups, plus the Reynolds number Re, which were varied during the course of the research.

Among the aforementioned governing parameters, the offset parameter E/D, is, perhaps, the most novel. The investigation of the effect of offset was deemed to be a relevant part of the research program because, in practice, precise alignment of the symmetry plane of the jet with the axis of the cylinder is unlikely. Three values of E/D were employed: 0, 0.5, and 1. The $E/D = 0$ case (no offset) is of interest in its own right and also serves as a baseline for assessing the effects of offset. When $E/D = 0.5$, the symmetry plane of the jet grazes the edge of the cylinder, while the $E/D = 1$ case offers the possibility of non-impingement of the jet on the cylinder.

For each of the aforementioned values of E/D, two nozzle widths, $W/D = 0.25$ and 0.5, were employed,

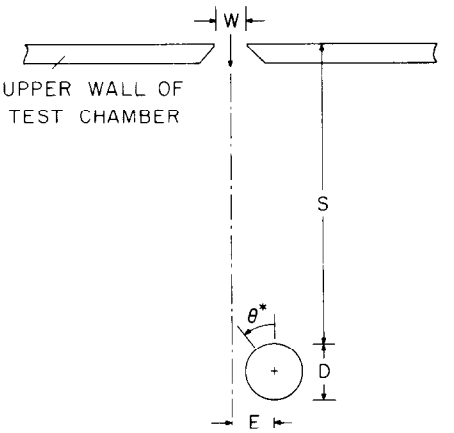

FIG. 1. Schematic diagram of the jet impingement configuration.

NOMENCLATURE

A_{slot}	slot inlet area
D	diameter of impingement cylinder
$\mathscr{D}$	mass diffusion coefficient
E	offset (Fig. 1)
K	mass transfer coefficient, $\dot{m}/(\rho_{nw}-\rho_{n\infty})$
$\dot{m}$	mass transfer per unit time and area
Nu	Nusselt number
$Nu_{0.7}$	Nusselt number for $Pr = 0.7$
Pr	Prandtl number
Re	Reynolds number, $\rho VD/\mu$
S	slot-to-cylinder separation distance (Fig. 1)
Sc	Schmidt number
Sh	Sherwood number
$Sh_{2.5}$	Sherwood number for $Sc = 2.5$
V	velocity at slot inlet
W	slot width (Fig. 1)
$\dot{w}$	flow rate in slot.

Greek symbols

θ^*	angle at impingement position (Fig. 1)
μ	viscosity
ν	kinematic viscosity
ρ	air density
ρ_{nw}	naphthalene vapor density at cylinder surface
$\rho_{n\infty}$	naphthalene vapor density in impinging jet.

and for each of these, the jet-origin to cylinder separation distance S/D was varied from $3\frac{1}{4}$ to $7\frac{1}{4}$ in increments of unity. The overall range of the Reynolds number extended from about 5000 to 60 000.

In addition to the heat transfer coefficient measurements, supplementary flow visualization studies were carried out using the oil–lampblack technique. These studies had two objectives. One was to verify the 2-D nature of the flow, while the other was to examine the pattern of jet impingement on the offset cylinder. In particular, the flow visualization provided information about the angle θ^* (illustrated in Fig. 1) at which the jet impinges on the surface of the cylinder.

In the available experimental literature on the impingement of a slot jet on a cylinder [2, 3], no consideration was given to jet-cylinder offset. Furthermore, in those studies, the jet was formed by a contoured nozzle rather than by a sharp-edged slotted plate as was employed here. The latter is much simpler to fabricate and should, therefore, have greater practical utility. In addition, the range of separation distances between the jet origin and the cylinder employed in refs. [2, 3] was appreciably different from that of the present experiments. The analysis of slot jet impingement set forth in ref. [4] provides stagnation point heat transfer coefficients but not circumferential-average values.

EXPERIMENTAL APPARATUS AND PROCEDURE

The heat transfer coefficients reported here were deduced from mass transfer measurements with the aid of the analogy between heat and mass transfer (to be elaborated later). The mass transfer experiments were performed using the naphthalene sublimation technique. Compared with heat transfer experiments, the naphthalene technique offers the advantages of significant apparatus simplifications, virtual absence of unaccounted extraneous losses, well-defined boundary conditions, and higher overall accuracy. The boundary condition for the mass transfer experiments corresponds to uniform wall temperature for the analogous heat transfer experiments.

Experimental apparatus

The impingement cylinder shown in a side view in Fig. 1 was 30.48 cm in overall length and 2.540 cm in diameter. It was a composite structure consisting of a solid rod, which formed the core of the cylinder, and three hollow-bore aluminum sleeves which, when slid end to end over the core, formed the outer surface of the cylinder. Of the three sleeves, one was centrally positioned with respect to the ends of the cylinder and served as the test section. The test section was flanked at each side by one of the other sleeves, thereby completing the cylinder. The lengths of the test section and of each flanking sleeve were 6.35 and 12.07 cm, respectively.

The test section was designed and fabricated to accommodate a coating of solid naphthalene. To this end, the central 5.08 cm of the 6.35 cm length of the test section was undercut on the diameter so as to form an annular recess. After the undercutting operation, the test section had a spool-like appearance. The pillar of the spool (i.e. the cylindrical surface produced by the undercutting) was roughened to aid in the adhesion of the naphthalene, which was implanted in the recess by a casting process, which will be described later. With the cast surface in place, the test section was of uniform outer diameter (2.540 cm) on both its naphthalene and metallic portions.

The temperature of the test section was measured by a fine-gauge (0.0254 cm), Teflon-coated, chromel–constantan thermocouple. The thermocouple was cast into the naphthalene coating with its junction situated about 0.025 cm from the exposed surface. The leads of the thermocouple passed into the bore of the test section and were drawn out to one end of the cylinder via an axial channel in the core rod. With its calibration, the thermocouple was accurate to 1 μV (0.017°C), which is the resolution of the voltmeter used to detect its e.m.f.

The impingement cylinder was housed in a large rectangular test chamber, 1.3 m high and having a square, horizontal cross-section of dimensions 0.67 $\times$ 0.67 m. The chamber was airtight, except for a narrow rectangular slot in its upper wall and an air exit port which was centered in its lower wall. The slot in the upper wall is pictured schematically in Fig. 1.

The system was operated in the suction mode, with air drawn into the slot from the temperature-controlled laboratory room. As noted earlier, the air streaming through the slot into the chamber forms a free jet which impinges in crossflow on the cylinder. Upon passing the cylinder, the air streams toward the bottom of the chamber, from which it exits into an air handling system consisting of a flowmeter (a calibrated rotameter), a control valve, and a blower. The blower was located in a service corridor outside the laboratory, and its compression-heated, naphthalene-enriched discharge was vented outside the building. This positioning ensured that the laboratory was free of naphthalene vapor.

As seen in Fig. 1, the downstream face of the slot was beveled back at an angle of 45° to allow for free separation of the flow (i.e. to avoid reattachment of the jet on the side walls of the slot). The 0.025 cm flat situated just forward of the bevel is standard in orifice-plate practice. Its purpose is to avoid possible warpage which might occur at a sharp-pointed beveled edge.

The upper wall of the test chamber was designed to enable the slot opening W to be easily varied. Two openings were employed, namely, $W = 0.250D$ and $0.500D$. The length of the slot in the direction normal to the plane of Fig. 1 was 22.86 cm. Thus, the aspect ratios (length/width) were 18 : 1 and 36 : 1, respectively, for the two slots employed during the research. These aspect ratios were sufficiently large to yield the desired two-dimensionality of the flow, as will be photographically documented when the results are presented.

The impingement cylinder was supported and positioned by fixtures attached to and suspended from the upper wall of the test chamber. The fixturing was designed so as not to interfere with the airflow. For the suspension of the cylinder, a pair of flat, vertical aluminum bars was employed, one to support each end of the cylinder. A vertical array of holes in the support bars was provided to enable the separation distance S (Fig. 1) to be varied in increments of 1.27 cm.

The upper end of each support bar was seated in a track-like channel bolted to the upper wall of the chamber. The channels served as guideways for the lateral displacement of the cylinder which gave rise to the offset E. To facilitate setting the offset, each channel was equipped with a precisely scribed scale and pointer.

Also suspended from the upper wall of the chamber was a pair of thin vertical plates, one adjacent to each of the aforementioned channels. The face of each plate was oriented perpendicular to the axis of the cylinder, and each was positioned so as to contact one of the ends of the cylinder. The plates were intended to minimize possible departures from two-dimensionality by inhibiting the lateral spreading of the jet (i.e. spreading along the direction of the cylinder axis). Experiments performed both with and without the baffle plates in place yielded virtually identical data. This finding indicated that even without the plates, the lateral spreading of the jet was too small to affect the flow over the test section.

For the proper execution of the experiment, it was necessary at various times to suppress sublimation from the naphthalene surface of the test section. For this purpose, a rapidly installable and rapidly removable test-section cover was fabricated from Delrin, a free machining plastic. The cover was a flexible sleeve with an integral clamp, the tightening of which completely suppressed mass transfer.

Experimental procedure

The first step in preparing for a data run was to cast a fresh naphthalene coating in the test section. Prior to the casting of the fresh coating, the naphthalene coating remaining from the preceding data run was removed from the test section by melting and evaporation. Then, the spool-like test section was placed on a flat surface so that it rested on one of its end faces and its axis was vertical. A brass sleeve whose inner diameter of 2.540 cm precisely matched the outer diameter of the test section was slipped over the spool. The bore of the brass sleeve had been polished and lapped to a high luster and was maintained in this state.

With the sleeve in place, the annular recess in the spool became a mold cavity. Molten naphthalene was poured into the cavity through an aperture in the upfacing end of the spool (a second aperture was provided for escape of air displaced by the naphthalene). Once the naphthalene had solidified, the sleeve was removed, exposing a naphthalene surface whose finish was comparable to that of the polished bore of the sleeve. The pouring and air-escape apertures were sealed with impermeable tape.

The more immediate preparations for a data run were begun with the assembly of the cylinder. The assembled cylinder, with the test section shrouded by the Delrin cover, was installed into the test chamber through an access window and, after the window was sealed, the airflow through the chamber was initiated and maintained. During the ensuing period, the output of the embedded thermocouple was carefully monitored. When a steady temperature was attained, the test section was removed from the test chamber, weighed (with the cover removed), and then returned to the chamber for a brief period of re-equilibration (with the cover on). Once a steady temperature was re-established, the protective cover was removed from the test section, and the data run proper was begun.

During the data run, the test section temperature was read periodically. The duration of the run was selected so as to limit the average sublimation-related recession of the naphthalene surface to less than 0.0025 cm. At the end of the run, the cylinder was disassembled (with the

cover on) and the test section subsequently weighed (with the cover removed).

The experiment was then continued in order to determine the amount of any extraneous mass transfer which might have occurred between the two weighings (e.g. during the setup and disassembly of the cylinder). To this end, all of the steps originally performed between the two weighings were repeated, but the naphthalene surface was not exposed to the airflow. Once this procedure had been completed, the test section was weighed again. The change of mass between this final weighing and the preceding weighing was employed as a subtractive correction (typically, less than 1%).

In addition to the test-section temperature, measurements were made of the rotameter float position and related pressure, the pressure in the test chamber, and the barometric pressure. The mass measurements were performed with a Sartorius ultra-precision, electronic analytical balance with a resolution of 10^{-5} g and a capacity of 166 g. Typically, about 0.1 g was sublimed during a data run.

The painstaking steps involved in the alignment of the cylinder are described elsewhere [5].

FLOW VISUALIZATION

As noted in the Introduction, visualization studies were performed to verify the two-dimensionality of the flow over the test section and to explore whether (and where) the offset jet impinged on the cylinder. The visualization was carried out with the aid of the oil–lampblack technique [6].

To use this technique, a mixture of lampblack powder and oil of suitable fluidity is prepared. The fluidity must be such that when the mixture is brushed on the surface of the cylinder, it will (a) not sag under the pull of gravity and (b) move over the surface in response to shear stresses exerted by the jet-driven fluid flow. Since condition (a) is best fulfilled by a stiff mixture while condition (b) requires an intermediate or light mixture (depending on the operating conditions), a compromise is necessary to more or less satisfactorily fulfill both conditions. The need for compromise leads to aesthetically less-than-perfect visualization patterns, but which provide the desired information.

It may also be noted that at a zone of low velocity (such as the stagnation line along which the jet impinges on the cylinder), the oil–lampblack mixture does not move. Since the entire surface of the cylinder was coated with a uniform film of the (black) mixture prior to the initiation of the airflow, the low velocity zones reveal themselves during the airflow period because they remain black.

To enable quantitative information to be obtained from the visualization experiments, the cylinder surface was covered with a sheet of white, plasticized, self-adhering contact paper prior to the application of the oil–lampblack mixture. Then, after the completion of the period of exposure of the cylinder to the airflow, the contact paper was removed from the cylinder and laid flat on a plane surface. The distance between the stagnation line and the upper apex of the cylinder was then measured using a precisely ruled scale ($\frac{1}{2}$ mm intervals), yielding the impingement angle θ^* (Fig. 1). Selected flow visualization patterns were photographed for record purposes.

A representative photograph of a visualization pattern is presented in Fig. 2. The figure corresponds to

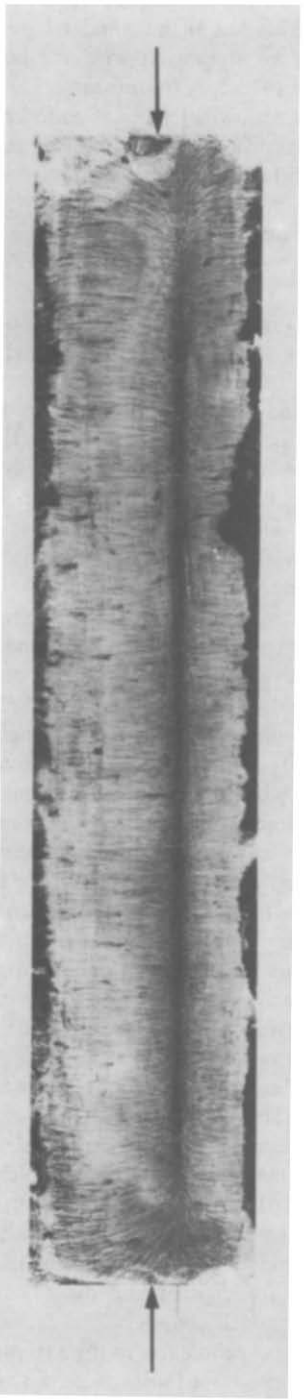

FIG. 2. Representative flow visualization pattern. The arrows mark the apex of the cylinder.

$E/D = 0.5$, $W/D = 0.5$, $S/D = 7.25$, and $Re = 31\,000$, but the qualitative features of the flow pattern displayed there are common to all the investigated cases.

The most prominent feature of Fig. 2 is the straight black line which runs nearly the entire length of the photograph. This is a stagnation line, which marks the locus along which the jet impinges head-on on the cylinder. Also shown in the figure is a pair of arrows, one at each end of the cylinder, marking the apex of the cylinder. The displacement of the stagnation line from the apex yields the impingement angle θ^* that is defined in Fig. 1. The impingement angle for Fig. 2 is 22.6° (a listing of θ^* values will be presented shortly).

The head-on collision documented by Fig. 2 (and by all the observed flow patterns) indicates that the jet follows a curved path from its origin to the surface of the offset cylinder.

Further inspection of Fig. 2 reveals the presence of fine streaklines which emanate from the stagnation line. These streaklines are perpendicular to the stagnation line, except near the ends of the cylinder. Thus, away from the ends, the streaklines reflect a circumferential (2-D) flow around the cylinder. The straightness of the stagnation line also testifies to the fact that most of the cylinder is free of end effects. In particular, the straight portion of the stagnation line is $9D$ in length, while the mass-transfer test section is $2D$ long. It may, therefore, be concluded that the mass transfer results obtained here are free of end effects and are equivalent to those for a cylinder of infinite length.

Along the vertical edges of Fig. 2, there are black bands. These bands indicate the beginning of the region of flow separation which extends around the remainder of the circumference of the cylinder.

Values of the impingement angle θ^* measured for offsets $E/D = 0.5$ and 1 are listed in Table 1. In interpreting the table, it may be noted that the smaller the impingement angle for a given offset, the greater is the bending of the jet.

Inspection of the table shows that for fixed values of the geometrical parameters, the impingement angle increases with increasing Reynolds number. This finding reflects the greater forward momentum of a high Reynolds number jet, which tends to inhibit its turning. Furthermore, for everything else fixed, θ^* decreases with increasing S/D, which is reasonable since more bending of the jet can take place over a longer path length. Also expected are the larger θ^* values at larger E/D. Less expected, however, is the insensitivity of θ^* to W/D for fixed values of S/D, E/D, and Re, but this can be rationalized by noting that fixed Re means fixed velocity (i.e. fixed momentum per unit mass).

Table 1. Impingement angle θ^* (degrees)

			Re		
W/D	E/D	S/D	1.5×10^4	3.1×10^4	6.0×10^4
0.25	0.5	3.25	27.1	29.3	31.6
		7.25	20.3	22.6	24.8
	1.0	3.25	38.4	45.1	51.9
		7.25	22.6	27.1	31.6
0.50	0.5	3.25	27.1	29.3	
		7.25	18.8	22.6	
	1.0	3.25	39.9	45.1	
		7.25	24.8	28.2	

Note that there are no data in Table 1 for $Re = 60\,000$ when $W/D = 0.5$. This is because that Reynolds number could not be attained with the available blower capacity. Also, for $Re < 15\,000$, definitive visualization patterns could not be obtained because the fluid shear was too low to cause decisive movements of the oil–lampblack mixture.

MASS (HEAT) TRANSFER RESULTS

Data reduction

The mass transfer $\dot{m}$ per unit time and unit area at the test section was evaluated from the defining relation $\dot{m} = \Delta M/\tau A_w$. On the RHS, ΔM is the amount of mass sublimed during a data run of duration time τ, and A_w is the surface area of the test section. The mass transfer is driven by the difference between the naphthalene vapor densities at the surface of the test section and in the jet, respectively, ρ_{nw} and $\rho_{n\infty}$. Correspondingly, the mass transfer coefficient K is defined as

$$K = \dot{m}/(\rho_{nw} - \rho_{n\infty}). \tag{1}$$

The quantity ρ_{nw} was determined by a two-step process. First, the naphthalene vapor pressure p_{nw} at the surface of the test section was calculated from the vapor pressure/temperature relation of ref. [7] using the measured surface temperature as input. Then, with p_{nw} and with the measured surface temperature, ρ_{nw} was obtained from the perfect gas law. For the conditions of the experiments, $\rho_{n\infty}$ was zero.

The dimensionless counterpart of the mass transfer coefficient is the Sherwood number, defined as

$$Sh = KD/\mathscr{D}. \tag{2}$$

To evaluate the diffusion coefficient $\mathscr{D}$, it is convenient to employ the Schmidt number Sc, so that $\mathscr{D} = \nu/Sc$. With this

$$Sh = (KD/\nu)Sc. \tag{3}$$

The kinematic viscosity appearing in equation (3) was evaluated as that for pure air, with the density corresponding to the measured pressure in the test chamber. Also, $Sc = 2.5$ for naphthalene diffusion in air [7].

The Reynolds number will be used to characterize the fluid flow aspects of the problem. The mass velocity ρV appearing in the Reynolds number was evaluated at the slot inlet, while the cylinder D was used as the characteristic dimension. This definition is consistent with that used in the prior experimental studies of slot jet impingement on a cylinder [2, 3]. If $\dot{w}$ is the rate of airflow passing through the slot and A_{slot} is the slot inlet area, then $\rho V = \dot{w}/A_{slot}$ and

$$Re = \rho VD/\mu = \dot{w}D/\mu A_{slot}. \tag{4}$$

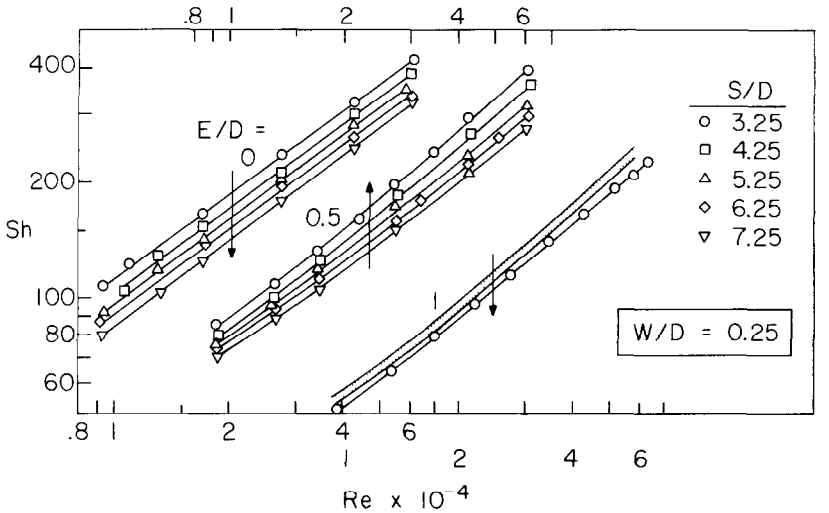

FIG. 3. Sherwood number results corresponding to the narrower slot ($W/D = 0.25$).

Heat/mass transfer analogy

The Sherwood number results obtained here can be readily transformed to Nusselt numbers appropriate to heat transfer applications. In this regard, the heat and mass transfer results presented in ref. [1] for various jet configurations were correlated in the form

$$Nu/Pr^{0.42} = Sh/Sc^{0.42} = f(Re, \chi_i) \quad (5)$$

where χ_i represents the geometrical parameters. The present Sherwood number results correspond to $Sc = 2.5$, so that

$$Nu = (Pr/2.5)^{0.42}\, Sh_{2.5}. \quad (6)$$

With the aid of equation (6), the Nusselt numbers for a heat transfer fluid with Prandtl number Pr can be determined from the Sherwood numbers presented here. In particular, for heat transfer between an air jet and a cylinder ($Pr \simeq 0.7$)

$$Nu_{0.7} = 0.586 Sh_{2.5}. \quad (7)$$

In view of equations (6) and (7), the terms heat transfer and mass transfer will be used interchangeably throughout the presentation of the results.

Sherwood (Nusselt) number results

Figures 3 and 4 convey the Sherwood number results for all of the four investigated parameters E/D, S/D, W/D, and Re. The $W/D = 0.25$ (narrower slot) results are presented in Fig. 3, while the results for $W/D = 0.5$ (wider slot) are in Fig. 4. Each figure consists of three groupings of data, respectively, from left to right, for the no-offset case ($E/D = 0$) and for the two offset cases ($E/D = 0.5$ and 1). For each E/D, data are presented for all five investigated distances between the jet origin and the cylinder ($S/D = 3.25$–7.25). Curves have been faired through the data to provide continuity.

In each figure, the Sherwood number is plotted as a function of the Reynolds number. To avoid overlap of the data for the different E/D, a different Reynolds

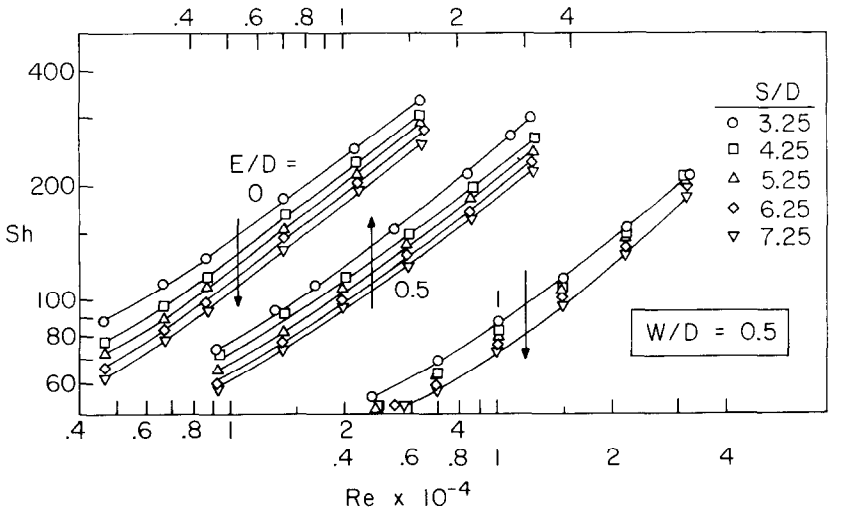

FIG. 4. Sherwood number results corresponding to the wider slot ($W/D = 0.5$).

number scale is used for each. The appropriate scale for each E/D is indicated by an arrow.

Attention may first be turned to Fig. 3. For the no-offset case, the Sherwood numbers for the various slot-to-cylinder separation distances S/D fall on straight lines that are nearly parallel ($Sh \sim Re^n$, with $n \simeq 3/4$). The Sherwood number decreases as the separation distance increases. This is consistent with the decrease in the jet velocity which occurs at increasing distances from the jet origin. The decrease of the Sherwood number with S/D is remarkably regular, with about a 7% dropoff between the successive lines of data.

With regard to the effect of offset, a comparison of the $E/D = 0.5$ and 1 data groupings with the $E/D = 0$ grouping indicates that offset acts to decrease the Sherwood number (note that the Reynolds number range is the same for all the E/D in Fig. 3). The actual extent of the reduction will be highlighted in a subsequent figure, but it can be seen from Fig. 3 that the decrease is not catastrophic. In particular, for the $E/D = 1$ offset, the jet issuing from the relatively narrow slot (i.e. $W/D = 0.25$) might have barely brushed the cylinder, resulting in very much reduced values of the Sherwood number. However, as observed from the flow visualization, the jet follows a curved path and impinges head-on on the cylinder. The head-on impingement moderates the offset-related reduction in the Sherwood number.

Turning to the specifics of the results for the offset cases in Fig. 3, it is seen that the Sh, Re distributions for $E/D = 0.5$, while smooth and regularly increasing with Re, are not straight, parallel lines as for the no-offset case. Rather, they are moderately curved and slightly divergent. This behavior is due, at least in part, to differences in the position of the impingement line (i.e. differences in θ^*) with Re and S/D.

For $E/D = 1$, the data for the various S/D are so close together that they are shown as a band rather than as individual points. The $S/D = 3.25$ (closest spacing) data fall slightly below the pack and are plotted separately. To rationalize these findings, it may be noted that the data are affected by two factors which vary oppositely with S/D. One of these is the decrease of the jet velocity with S/D. The other is the increase in the size of the zone of separation-free flow on the cylinder which accompanies an increase in S/D when $E/D = 1$ (as observed from the visualization patterns for $E/D = 1$). The conflict between these two effects is believed responsible for the narrow spread of the data with S/D. The relatively low Sh values for $S/D = 3.25$ may be attributed to the dominance of flow separation effects for that case.

Consideration will now be given to Fig. 4, which corresponds to the wider of the two slots. Owing to the wider slot, the *effective* offset for a given value of E/D is smaller than that for Fig. 3. As a result, it is reasonable to expect smaller offset-related effects in Fig. 4 than in Fig. 3. A comparison of the figures confirms this expectation. The $E/D = 0.5$ distributions are only moderately different from those for $E/D = 0$. Greater differences are in evidence for $E/D = 1$, but the data for the various S/D are distinct, and their ordering with S/D is the same as for $E/D = 0$ and 0.5.

Another difference between Figs. 3 and 4 is in their Reynolds number ranges. In particular, the data in Fig. 4 extend to lower Reynolds numbers than those of Fig. 3. In this extended range, the Sh distributions for the no-offset case in Fig. 4 display moderate curvature. However, for $Re > 9000$ (the starting point of the Re range of Fig. 3), these distributions are straight and virtually parallel. They are described by the relation $Sh \sim Re^n$, where $n \simeq 3/4$. This is exactly the same relation (same n value) which described the no-offset results presented in Fig. 3. Thus, for the no-offset case,

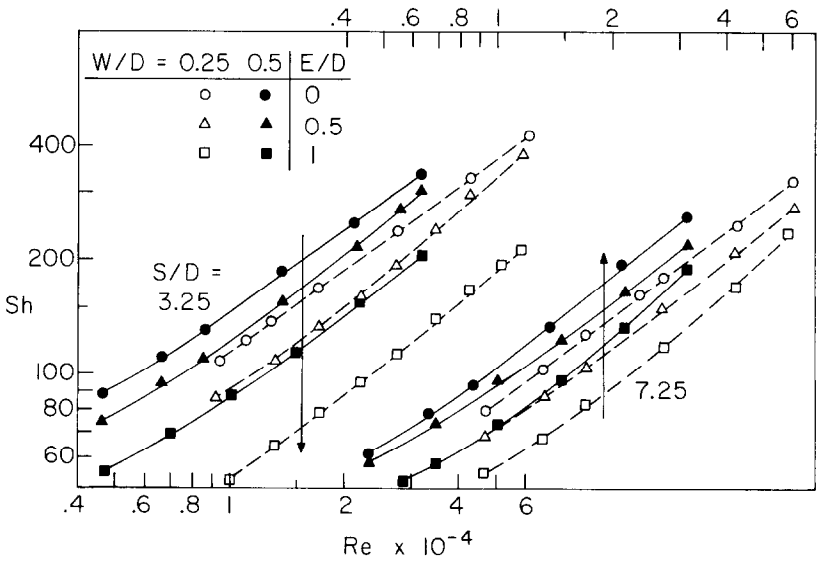

FIG. 5. Sherwood number presentation highlighting the effects of offset.

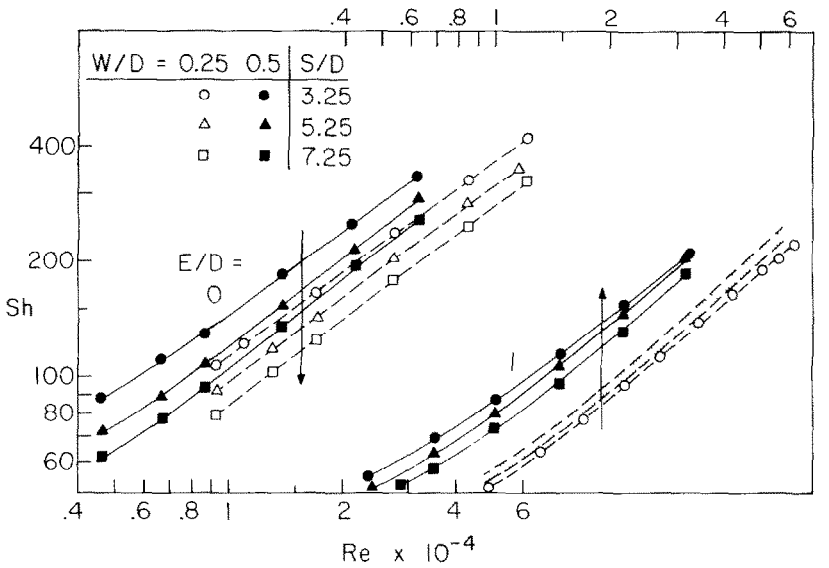

FIG. 6. Sherwood number presentation highlighting the effects of slot width.

the Reynolds number dependence of the Sherwood number results is virtually independent of S/D and of W/D in the investigated ranges.

To facilitate a more quantitative appraisal of the effects of offset, Fig. 5 has been prepared. The grouping of data at the left of the figure is for $S/D = 3.25$, while that at the right is for $S/D = 7.25$ (respectively, the smallest and largest slot-to-cylinder spacings). Within each grouping, there are six sets of data, three for $W/D = 0.25$ (open symbols) and three for $W/D = 0.5$ (black symbols). The three sets of data for each W/D correspond to $E/D = 0$, 0.5, and 1.

Attention will first be focused on the results for $S/D = 3.25$. For each fixed slot width W/D, the Sherwood number is seen to decrease as E/D increases from 0 to 0.5 to 1. The extent of the decrease between $E/D = 0.5$ and 1 is markedly greater than that between $E/D = 0$ and 0.5. It is also evident that for a given E/D offset, the reduction in the Sherwood number (relative to that for $E/D = 0$) is more marked when the slot is narrower. Thus, for $E/D = 1$, the Sherwood number is 50–55% lower than that for $E/D = 0$ when $W/D = 0.25$; however, when $W/D = 0.5$, the Sherwood number is about 40% below that for $E/D = 0$. This confirms the earlier assertion that the effective offset diminishes with increasing slot width.

The results for $S/D = 7.25$ are seen to be more tightly grouped than are those for $S/D = 3.25$, thereby testifying to the diminished effect of offset as S/D increases. For example, the aforementioned 50–55% decrease in Sh at $S/D = 3.25$ for $E/D = 1$ and $W/D = 0.25$ becomes a 30% decrease at $S/D = 7.25$. As discussed earlier, this behavior is due to the increase in size of the zone of separation-free flow over the offset cylinder as S/D increases.

Figure 5 also facilitates a comparison between the magnitudes of the Sherwood numbers for the two slot widths $W/D = 0.25$ and 0.5. It is evident that for a fixed Reynolds number and fixed values of S/D and E/D, the Sherwood number is larger for wider slots. This finding may be made plausible by noting that a fixed Reynolds number implies a fixed velocity of the jet, but that the mass flow increases in proportion to the width of the slot. It is this factor which yields the higher Sherwood numbers for the wider slot.

A final perspective on the Sherwood number results is provided by Fig. 6. This figure is a selective combination of Figs. 3 and 4, thereby facilitating their quantitative comparison. The results for $W/D = 0.25$ are represented by open symbols, while those for $W/D = 0.5$ are depicted by black symbols. The data are grouped according to offset—$E/D = 0$ at the left and $E/D = 1$ at the right.

Figure 6 confirms the higher Sherwood numbers provided by the wider slot. It is also seen from the figure that for a fixed slot-to-cylinder separation distance and a fixed Reynolds number, the spread of the data with W/D is greater for $E/D = 1$ than for $E/D = 0$. Thus, the sensitivity of the results to slot width increases with increasing E/D. This is due, at least in part, to the fact that the slot width influences the effective offset, so that for a given nominal offset E/D, the effective offsets corresponding to different slot widths will differ.

CONCLUDING REMARKS

The crossflow impingement of a slot jet on a circular cylinder has been studied here using the naphthalene sublimation technique. The experimentally determined Sherwood numbers can be converted to Nusselt numbers by using the analogy between heat and mass transfer as set forth by equations (6) and (7).

The experiments were performed for parametric variations of four dimensionless quantities. Among these, the geometric parameters included E/D, S/D, and W/D, where E is the offset of the cylinder axis from the

symmetry plane of the slot, S is the distance between the slot and the cylinder surface, W is the slot width, and D is the cylinder diameter. The fourth parameter is the Reynolds number.

The offsetting of the cylinder from the symmetry plane of the jet was one of the special features of the research. Another feature was the use of a sharp-edged slotted plate to create the jet. This configuration is simpler to fabricate than the contoured nozzles used in prior studies and should, therefore, have greater practical utility.

The mass transfer experiments were supplemented by flow visualization studies performed with the oil–lampblack technique. The visualization experiments demonstrated that the flow over the test section was free of end effects and was two-dimensional. In the presence of offset, the jet follows a curved path in order to impinge head-on on the cylinder. The locations at which the jet impinged on the offset cylinder are listed in Table 1.

For the no-offset case, the Sherwood numbers obey the power law $Sh \sim Re^n (n \simeq 3/4)$ for $Re > 9000$, which is a straight line on logarithmic coordinates. In the presence of offset, the Sh, Re distributions display moderate curvature.

The Sherwood numbers were found to increase with slot width, and the sensitivity of the results to slot width increased with increasing offset. The Sherwood numbers generally decreased with increasing slot-to-cylinder separation distance, but at large offsets the results were relatively insensitive to the separation distance.

Offset acts to decrease the Sherwood number. The extent of the decrease is magnified at larger offsets, and the effect of the offset also becomes more marked for narrower jets. Furthermore, the offset effect is greatest at small slot-to-cylinder separation distances and decreases as the separation distance increases. The largest measured offset-related reduction in the Sherwood number was slightly in excess of 50%.

REFERENCES

1. H. Martin, Heat and mass transfer between impinging gas jets and solid surfaces, in *Advances in Heat Transfer*, Vol. 13, pp. 1–60. Academic Press, New York (1977).
2. M. Kumada, I. Mabuchi and Y. Kawashima, Mass transfer on a cylinder in the potential core region of a two-dimensional jet, *Heat Transfer–Jap. Res.* **2**(3), 53–66 (1973).
3. H. Schuh and B. Persson, Heat transfer on circular cylinders exposed to free-jet flow, *Int. J. Heat Mass Transfer* **7**, 1257–1271 (1964).
4. H. Miyazaki and E. M. Sparrow, Potential flow solution for crossflow impingement of a slot jet on a circular cylinder, *J. Fluids Engng* **98**, 249–255 (1976).
5. A. Alhomoud, Heat transfer from a circular cylinder due to slot jet impingement, Ph.D. thesis, Department of Mechanical Engineering, University of Minnesota, Minneapolis, Minnesota (1984).
6. W. Merzkirch, *Flow Visualization*, pp. 53–56. Academic Press, New York (1974).
7. H. H. Sogin, Sublimation from discs to air streams flowing normal to their surfaces, *Trans. Am. Soc. Mech. Engrs* **80**, 61–71 (1958).

TRANSFERT THERMIQUE A L'IMPACTION SUR UN CYLINDRE CIRCULAIRE D'UN JET PLAN FRONTAL CENTRE OU NON

Résumé—On mesure des coefficients de transfert thermique sur un cylindre soumis à l'impact d'un jet plan. Dans une série d'expériences le plan de symétrie du jet contient l'axe du cylindre, tandis que dans une autre le jet est décalé. Des variations paramétriques sont faites pour la largeur du jet, la distance entre la sortie du jet et le cylindre, et le nombre de Reynolds. Des visualisations montrent que, même en présence du décalage, le jet frappe le cylindre mais pas à son sommet comme dans le cas aligné. On trouve que le coefficient de transfert croît avec la largeur de la fente et le nombre de Reynolds, mais diminue avec la distance fente–cylindre et le décalage. L'effet du décalage est accentué pour des fentes étroites et des petites distances fente–cylindre. La plus grande réduction du coefficient de transfert thermique mesurée pour un décalage dépasse légèrement 50%.

DER WÄRMEÜBERGANG AN EINEM KREISRUNDEN ZYLINDER AUFGRUND EINES VERSETZT ODER FLUCHTEND AUFTREFFENDEN SPALTSTRAHLS

Zusammenfassung—Es wurden Wärmeübergangskoeffizienten an einem kreisrunden Zylinder, der einem im Kreuzstrom auftreffenden Spaltstrahl ausgesetzt war, gemessen. In einem Teil der Versuche war die Symmetrieebene des Strahls fluchtend zur Zylinderachse, während im anderen Teil der Strahl bezüglich des Zylinders versetzt war. Außer der Strahlversetzung wurden weitere Parametervariationen für die den Strahl erzeugende Spaltbreite, den Abstand zwischen Spalt und Zylinder und die Reynolds-Zahl durchgeführt. Versuche zur Sichtbarmachung der Strömung ergaben, daß der Strahl trotz Versetzung auf den Zylinder aufprallt, wenn auch nicht am Zylinderscheitel wie im fluchtenden Fall. Es zeigte sich, daß der Wärmeübergangskoeffizient mit der Spaltbreite und der Reynoldszahl zunimmt, bei wachsendem Abstand zwischen Spalt und Zylinder sowie größerer Versetzung jedoch abnimmt. Der Einfluß der Versetzung ist für enge Spalte und kleineren Abstand zwischen Spalt und Zylinder besonders ausgeprägt. Die größte durch Versetzung gemessene Reduzierung der Wärmeübergangskoeffizienten lag knapp über 50%.

ТЕПЛОПЕРЕНОС ПРИ ОБТЕКАНИИ КРУГЛОГО ЦИЛИНДРА СТРУЯМИ, ИСТЕКАЮЩИМИ ИЗ СМЕЩЕННОЙ ИЛИ НЕСМЕЩЕННОЙ ОТНОСИТЕЛЬНО ЦИЛИНДРА ЩЕЛИ

Аннотация—Измерены коэффициенты теплопереноса для круглого цилиндра при поперечном обтекании истекающей из щели струей. В одной серии экспериментов плоскость симметрии струи совмещалась с осью цилиндра, а в другой струя смещалась относительно цилиндра. Кроме ширины щели варьировались также расстояние между щелью и цилиндром и число Рейнольдса. Дополнительные эксперименты по визуализации течения показали, что даже при смещении струя попадает на цилиндр, хотя и не в той части, как в случае без смещения. Найдено, что коэффициент теплопереноса растет с увеличением ширины щели и числа Рейнольдса, но снижается с ростом расстояния между щелью и цилиндром и степенью смещения. Влияние смещения более заметно для узких щелей и малых расстояний между щелью и цилиндром. Наибольшее снижение коэффициента теплопереноса за счет смещения составило более 50%.